FLUORINE CHEMISTRY

Handling fluorinated gases as solid reagents using metal-organic frameworks

Kaitlyn T. Keasler[1], Mary E. Zick[1]†, Emily E. Stacy[1]†, Jaehwan Kim[1], Jung-Hoon Lee[2], Lida Aeindartehran[3], Tomče Runčevski[3], Phillip J. Milner[1]*

Fluorine is an increasingly common substituent in pharmaceuticals and agrochemicals because it improves the bioavailability and metabolic stability of organic molecules. Fluorinated gases represent intuitive building blocks for the late-stage installation of fluorinated groups, but they are generally overlooked because they require the use of specialized equipment. We report a general strategy for handling fluorinated gases as benchtop-stable solid reagents using metal-organic frameworks (MOFs). Gas-MOF reagents are prepared on gram-scale and used to facilitate fluorovinylation and fluoroalkylation reactions. Encapsulation of gas-MOF reagents within wax enables stable storage on the benchtop and controlled release into solution upon sonication, which represents a safer alternative to handling the gas directly. Furthermore, our approach enables high-throughput reaction development with these gases.

Fluorinated organic molecules account for 20 to 30% of active pharmaceutical ingredients and >40% of agrochemicals owing to their improved metabolic stabilities and membrane permeabilities compared with their nonfluorinated analogs (Fig. 1A) (*1*–*6*). In addition, ^{18}F-labeled compounds are prominent radiotracers for positron emission tomography (*7*). Despite the importance of fluorine across numerous fields, the selective, late-stage introduction of fluoroalkyl and fluorovinyl groups into drug-like molecules remains a frontier in organic synthesis (*8*–*10*). Simple fluorinated commodity chemicals such as vinylidene fluoride (VDF), trifluoropropene (TFP), hexafluoropropene (HFP), and trifluoromethyl iodide (TFMI) represent inexpensive potential building blocks for the installation of fluoroalkyl and fluorovinyl groups (Fig. 1B). For example, VDF and TFP provide entry points for the synthesis of fluorinated alkenes, which are important bioisosteres for carbonyl groups in medicinal chemistry. As such, VDF has the potential to substantially streamline the synthesis of complex fluorinated molecules such as 5-(2,2-difluorovinyl)-2′-deoxyuridine (Fig. 1C) (*6*). However, these reagents remain underutilized because they are gases at room temperature (RT) and pressure. The use of gaseous reagents necessitates specialized equipment for safe handling (*11*, *12*). Fluorinated gases are also generally toxic, flammable, ozone depleting, and/or otherwise environmentally destructive (*13*), making them challenging to use for high-throughput reaction discovery. As such, a general strategy for safely using fluorinated gases would greatly facilitate the synthesis of fluorinated molecules that are relevant to medicinal chemistry, agriculture, biomedical imaging, and beyond.

The use of gaseous reagents in organic synthesis generally requires handling the gas directly (e.g., filling a balloon from a cylinder; Fig. 1D, left) or generating the gas in situ or ex situ from stable molecular precursors (Fig. 1D, center) (*14*–*17*). Both strategies suffer from key limitations. The former is simple, but it is low throughput, lacks stoichiometric control, and produces substantial gas waste, an issue that is

[1]Department of Chemistry and Chemical Biology, Cornell University, Ithaca, NY 14850, USA. [2]Computational Science Research Center, Korea Institute of Science and Technology (KIST), Seoul 02792, Republic of Korea. [3]Department of Chemistry, Southern Methodist University, Dallas, TX 75275, USA. *Corresponding author. Email: pjm347@cornell.edu
†These authors contributed equally to this work.

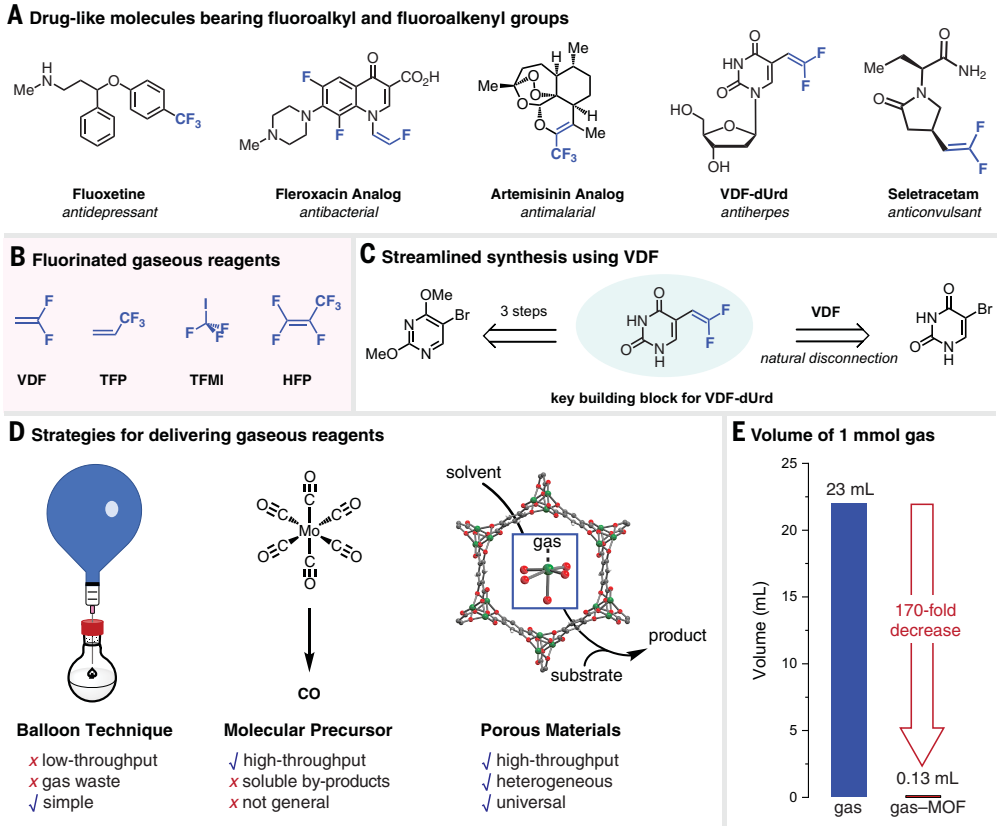

Fig. 1. Delivery of fluorinated gases using MOFs. (**A**) Examples of drug-like molecules bearing fluoroalkyl and fluoroalkenyl groups. dUrd, 2′-deoxyuridine; Me, methyl. (**B**) Fluorinated gaseous building blocks. (**C**) Streamlined synthesis using VDF (*6*). (**D**) Overview of gas-reagent delivery strategies, including balloons, generation from molecular precursors, and release from porous materials (this work). (**E**) The volume of 1 mmol of an ideal gas compared with 1 mmol of gas contained in a MOF [Mg_2(dobdc) with a crystallographic density of 0.909 g/cm^3 (*73*, *74*) and one gas molecule per metal site].

exacerbated with toxic and environmentally destructive gases. Although the latter approach is amenable to high-throughput screening, it requires the design of a new delivery strategy for each gas and results in soluble by-products that must be separated from the desired products. We hypothesized that the reversible adsorption of fluorinated gases within porous solids should allow for their facile handling as recyclable solid reagents, overcoming the limitations outlined above and facilitating the development of methods for fluorinating complex molecules (Fig. 1D, right). Among porous solids, metal-organic frameworks (MOFs), which are crystalline materials constructed from organic linkers and inorganic nodes, are distinctively modular, allowing for the optimization of storage capacity and enthalpy of adsorption ($-\Delta H_{ads}$) for any gas of interest (*18*–*20*). In particular, MOFs that bear coordinatively unsaturated metal centers (open metal sites) (*21*) should reversibly bind synthetically relevant fluorinated gases through strong metal-fluorine (M-F) interactions (*22*, *23*). Owing to the high theoretical gravimetric and volumetric capacities of MOFs such as Mg_2(dobdc) (dobdc^{4-} is 2,5-dioxidobenzene-1,4-dicarboxylate) (*24*), 1 mmol (23 ml) of gas can be delivered with as little as 120 mg (0.13 ml) of MOF, resulting in a staggering ~170-fold volume reduction compared with a free ideal gas (Fig. 1E). In this work, we demonstrate that the commodity fluorinated gases VDF, TFP, HFP, and TFMI can be stored within MOFs and handled as solid reagents, enabling their facile use in otherwise challenging fluoroalkylation and fluorovinylation reactions.

Selection of the optimal MOF for fluorinated gas storage

To be useful for controlled fluorinated gas delivery, a porous material should possess a high gas sorption capacity, interact strongly with a range of fluorinated gases to prevent undesired gas leakage, and be stable toward long-term storage on the benchtop. Given the scarcity of available data regarding the adsorption of fluorinated commodity chemicals within porous solids, we commenced by studying VDF uptake in 12 representative open-metal-site MOFs, including HKUST-1 or $Cu_3(btc)_2$ (btc^{3-} is benzene-1,3,5-tricarboxylate) (*25*), MIL-100(Fe) or $Fe_3(O)(OH)(btc)_2$ (*26*), NH_2-MIL-101(Al) or $Al_3(O)(OH)(NH_2\text{-bdc})_3$ (NH_2-bdc^{2-} is 2-aminobenzene-1,4-dicarboxylate) (*27*), MOF-74 or M_2(dobdc) (M is Mg, Mn, Fe, Co, Ni, Cu, or Zn) (*28*), and *m*-MOF-74 or M_2(*m*-dobdc) (M is Mg or Ni; *m*-dobdc^{4-} is 4,6-dioxidobenzene-1,3-dicarboxylate) (*29*) (see fig. S2 for structures). We also investigated one commercially available zeolite that bears accessible Na^+ sites (Zeolite Y). To identify the optimal material for fluorinated gas delivery, VDF adsorption and desorption isotherms were collected for all materials at 30°, 40°, and 50°C. Notably, VDF adsorption was found to be fully reversible in every case. The isotherm data were used to determine the gravimetric VDF storage capacities at 30°C and 1 bar of VDF (vertical axis of Fig. 2A, fig. S80, and table S23). Among the tested materials, Mg_2(dobdc) (7.95 mmol/g, 34 wt %) and $Cu_3(btc)_2$ (7.64 mmol/g, 33 wt %) possess the highest VDF gravimetric capacities, which is expected given their high densities of open metal sites and low molecular weights. Beyond storage capacity, the enthalpy of adsorption ($-\Delta H_{ads}$) is critical for governing how readily fluorinated gases would be released in situ or under ambient conditions. To calculate $-\Delta H_{ads}$ values, all adsorption isotherms were fit using dual-site Langmuir models. Using the Clausius-Clapeyron equation, we determined the $-\Delta H_{ads}$ values as a function of VDF loading for each material; $-\Delta H_{ads}$ values at a loading of 1 mmol/g are included for comparison in Fig. 2A (horizontal axis). In general, materials that bear highly Lewis acidic Mg^{2+}, Ni^{2+}, or Na^+ sites—namely M_2(dobdc) (M is Mg or Ni), M_2(*m*-dobdc) (M is Mg or Ni), and Zeolite Y—demonstrate the

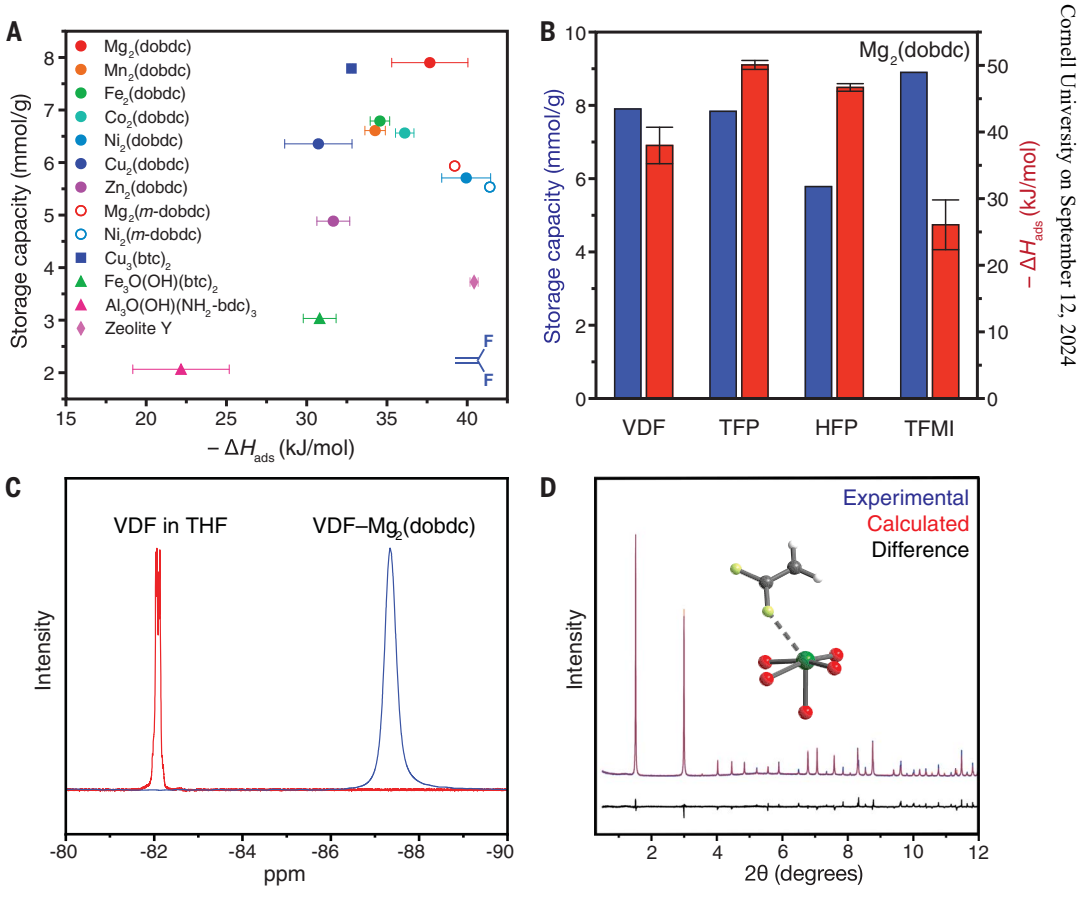

Fig. 2. Fluorinated gas adsorption in open-metal-site materials. (**A**) Comparison of storage capacity and binding enthalpy for VDF in porous materials. The binding enthalpies and associated errors were determined using linear fits to the Clausius-Clapeyron equation. (**B**) Comparison of storage capacity (blue) and binding enthalpy (red) for fluorinated gases in Mg_2(dobdc). The binding enthalpies and associated errors were determined using linear fits to the Clausius-Clapeyron equation. (**C**) MAS ^{19}F solid-state NMR spectrum of VDF-Mg_2(dobdc) (blue) compared with solution-state ^{19}F NMR spectrum of VDF in THF (red). (**D**) Rietveld refinement of VDF-Mg_2(dobdc). Measured diffraction data (blue), fitted pattern (red), and the difference (black) are shown. Weighted residual factor (R_{wp}) = 11.9%. The inset shows the structural model for VDF-Mg_2(dobdc).

strongest adsorption of VDF (38 to 41 kJ/mol). This is likely due in part to the hard-soft acid-base match of hard fluorine atoms with hard metal centers (*22*).

Because Mg_2(dobdc), Ni_2(dobdc), and Ni_2(*m*-dobdc) display high VDF gravimetric storage capacities coupled with strong binding, their ability to adsorb the fluorinated gases TFP, HFP, and TFMI was also evaluated (Fig. 2B, fig. S81, and table S24). Because of its lower molecular weight, Mg_2(dobdc) exhibits a higher gravimetric capacity for each gas at 1 bar and 30°C than Ni_2(dobdc) and Ni_2(*m*-dobdc). In addition, the $-\Delta H_{ads}$ values for TFP and TFMI in Mg_2(dobdc) are larger in magnitude than the corresponding values in the Ni-based frameworks, whereas the strength of HFP binding is comparable across all three frameworks. Collectively, the adsorption data suggest that Mg_2(dobdc) is an ideal framework for the storage of fluorinated gases because of its high gravimetric capacity and strong interaction with multiple gases of synthetic interest. Further supporting its superiority as a practical gas storage medium, Mg_2(dobdc) retains its crystallinity and porosity after a week of standing on the benchtop at RT (figs. S93 and S94) and is stable in air at 120°C for 24 hours (*30*). To demonstrate the potential for commercialization of Mg_2(dobdc), we developed a new high-concentration aqueous synthesis that allows for >100 g of material to be prepared in a single batch (figs. S10 and S11).

The nature of the interaction between Mg_2(dobdc) and VDF (as a representative fluorinated gas) was probed using a range of experimental and computational techniques (Fig. 2, C and D; figs. S82 and S96; and table S25). Magic-angle spinning (MAS) ^{19}F solid-state nuclear magnetic resonance (NMR) measurements were performed on VDF-Mg_2(dobdc) (Fig. 2C and fig. S96). The resonance corresponding to VDF-Mg_2(dobdc) [−87.34 parts per million (ppm)] is shifted upfield and broadened relative to that of VDF dissolved in tetrahydrofuran (THF) (−82.09 ppm) (Fig. 2C and fig. S96). The greater shielding that is observed for VDF bound within the MOF is due to the proximity of π electron density from the aromatic linkers, and the signal broadening is due to immobilization (*22*, *31*). The preferred binding mode of VDF in Mg_2(dobdc) was further interrogated by synchrotron powder x-ray diffraction (PXRD) conducted on a sample of microcrystalline Mg_2(dobdc) dosed with ~100 mbar of VDF (Fig. 2D). Rietveld refinement of the obtained pattern corroborated a structural model in which VDF preferentially binds to the open Mg^{2+} site through a F···Mg interaction, not through the alkene π-bond (inset of Fig. 2D). The F···Mg distance is 2.67(3) Å, which is similar to the distances reported for related experimental and calculated structures (*22*, *23*). Density functional theory calculations further support that the F-bound structure for VDF-Mg_2(dobdc) possesses a predicted binding enthalpy ($-\Delta H_b$ = 37.5 kJ/mol) similar to the experimental value ($-\Delta H_{ads}$ = 37.7 kJ/mol) (fig. S82 and table S25). Indeed, the calculated F-bound structures for TFP, HFP, and TFMI all possess predicted binding enthalpies that are similar to the experimental values (fig. S82 and table S25). Overall, these data support that the strong binding of fluorinated gases in Mg_2(dobdc) is due to the favorable interaction between the hard Lewis basic F atoms and the hard Lewis acidic Mg^{2+} open metal sites in Mg_2(dobdc).

Application to solution-phase reactions

Building on these results, we investigated whether gas-Mg_2(dobdc) reagents can be used to deliver fluorinated gases under synthetically relevant conditions. Activated Mg_2(dobdc) was dosed with VDF, and the resulting gas-MOF reagent was loaded into a custom-built, air-free solid-addition funnel to enable controlled delivery into solution (Fig. 3A). ^{19}F NMR analysis confirmed that this approach facilitates rapid VDF release into solvents of varying polarity within 10 min (Fig. 3A and figs. S89 to S92). To further control the kinetics of gas release into solution, we loaded VDF-Mg_2(dobdc) into a gas-tight wax capsule (fig. S87) (*32*). When the encapsulated VDF-Mg_2(dobdc) was suspended in *N*,*N*-dimethylformamide (DMF), no VDF was detected in solution after an hour. This result suggests that the wax capsules are impermeable to VDF, representing a leak-proof encapsulation strategy. Simple sonication of the reaction mixture breaks the capsule open and dispenses VDF-Mg_2(dobdc), triggering the complete discharge of VDF into solution. These practical, single-use reagents enable high-throughput screening of reactions involving gases while preventing direct exposure to the gas and circumventing the need for complex equipment (*11*, *12*).

To explore the utility of gas-MOF reagents in synthetic chemistry, we envisioned that a desirable yet unrealized transformation would be the defluorinative coupling of VDF with easily handled (hetero)aryl nucleophiles to yield α-fluorostyrenes (*33*). Owing to their topological, electronic, and steric similarities (*34*), monofluoroalkenes have been widely used as amide bioisosteres in drug and peptidomimetic design (*34*–*36*). Traditional synthetic routes to access terminal α-fluoroalkenes through alkyne or alkene functionalization pathways suffer from key drawbacks such as multistep starting material syntheses, harsh or hazardous reaction conditions, poor regioselectivity, and/or modest scopes (*37*–*39*). Meanwhile, previously reported metal-catalyzed cross-coupling routes to prepare α-fluorostyrenes require air-sensitive starting materials and/or specialized equipment to handle gaseous VDF (*40*–*44*). To design a more streamlined protocol, we used VDF-Mg_2(dobdc) to enable a base-free, defluorinative Suzuki-Miyaura coupling (*45*) with (hetero)aryl boronic acids (Fig. 3B), representing a straightforward route to access α-fluorostyrenes. Without the need to handle gaseous reagents, we simply combined 4-biphenylboronic acid and VDF-Mg_2(dobdc) at RT using palladium trifluoroacetate [$Pd(TFA)_2$] as the catalyst, 4,4′-di-tert-butyl-2,2′-bipyridine (dtbbpy) as the ligand, and DMF as the solvent to obtain the α-fluorostyrene product in 23% yield (table S26, entry 1). Although reactions that involve reactive gases are typically low throughput, using VDF-Mg_2(dobdc) enables the setup of multiple reactions in parallel, streamlining the optimization process (table S26). An investigation of catalysts, solvents, temperatures, and concentrations revealed that the use of catalytic $Pd(TFA)_2$(dtbbpy) and a reaction concentration of 50 mM (with respect to the arylboronic acid) leads to nearly quantitative yield (table S26, entry 23). Critically, the equivalents of VDF can be adjusted by modifying the amount of VDF-Mg_2(dobdc) added to the reaction; doing so revealed that the reaction proceeds well using either four or eight equivalents of VDF (table S26, entries 23 and 24). The optimized defluorinative coupling protocol proceeds smoothly with a variety of (hetero)arylboronic acid substrates, furnishing the α-fluorostyrene products in good isolated yields (Fig. 3B). We obtained comparable yields using either freshly prepared VDF-Mg_2(dobdc) dispensed from a gas-tight solid-addition funnel or wax-encapsulated VDF-Mg_2(dobdc) reagents after a day of storage on the benchtop. After a successful reaction, the MOF was recovered and found to retain its crystallinity by PXRD, suggesting that it can potentially be recycled (fig. S95). Using a balloon of VDF in place of VDF-Mg_2(dobdc) affords the product in slightly lower yield [67% compared with 80% with VDF-Mg_2(dobdc)], demonstrating that our strategy is competitive with conventional gas delivery techniques. Given the simplicity of the protocol reported herein, we expect that it will find broad use for the synthesis of functionalized α-fluorostyrenes.

Scattered reports in the literature suggest that the coupling of HFP with aryl magnesium bromides (*46*) or arylboronic acid neopentylglycol esters (*47*) results in mixtures of stereo- and regioisomers. We sought to expand the scope of our defluorinative coupling of VDF and commercially available (hetero)arylboronic acids (Fig. 3B) to achieve a similar reaction using HFP-Mg_2(dobdc). Our preliminary efforts led to the defluorinative coupling of HFP and 4-biphenylboronic acid to furnish a 1:1 *E*:*Z* mixture of pentafluoropropene-substituted products (Fig. 3C). This result demonstrates how the use of gas-MOF reagents enables reaction development with multiple gases without needing to change cylinders attached to complicated manifolds.

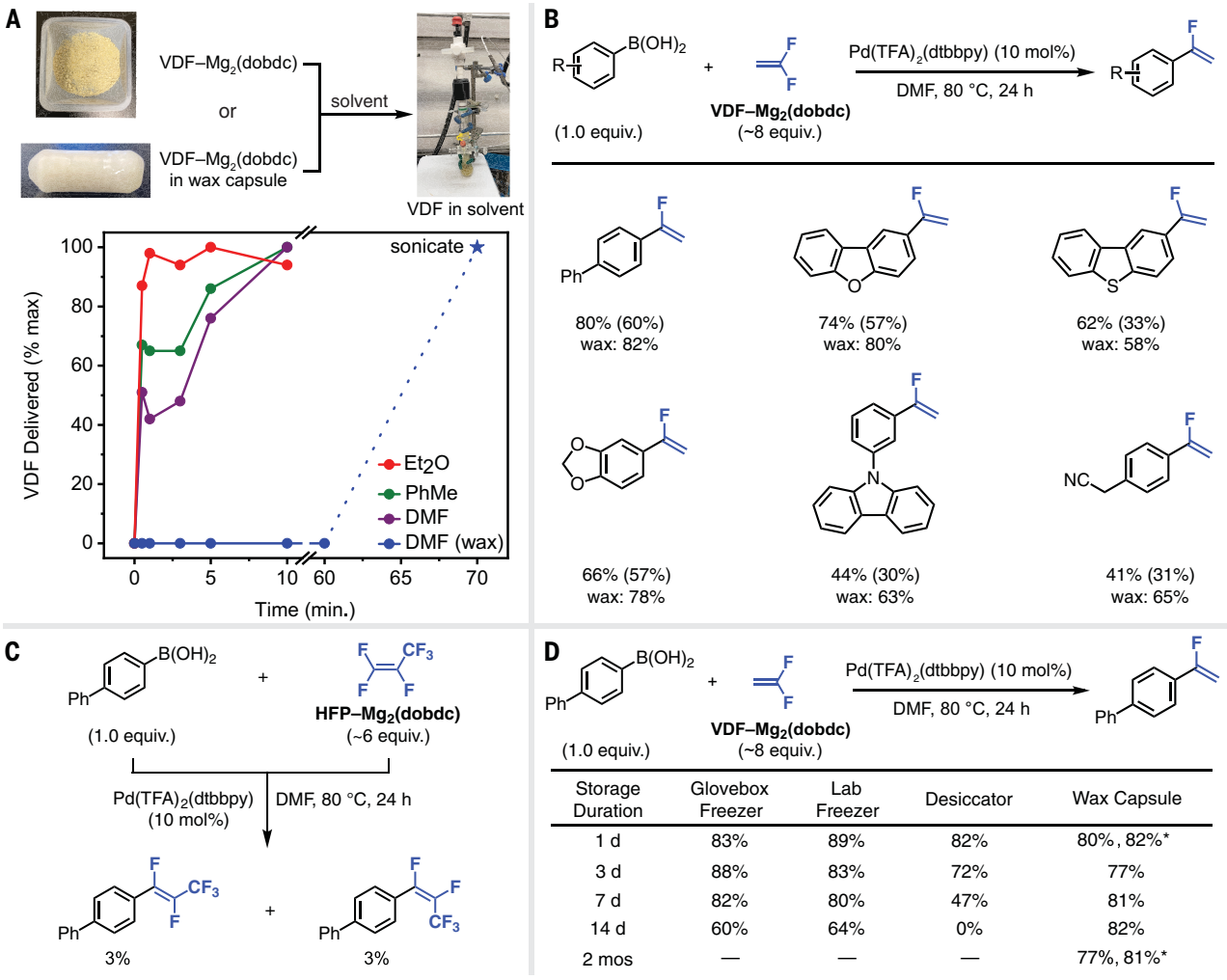

Storage Duration	Glovebox Freezer	Lab Freezer	Desiccator	Wax Capsule
1 d	83%	89%	82%	80%, 82%*
3 d	88%	83%	72%	77%
7 d	82%	80%	47%	81%
14 d	60%	64%	0%	82%
2 mos	—	—	—	77%, 81%*

Fig. 3. Delivery and synthetic transformations of VDF and HFP. NMR yields were determined by ^{19}F NMR integration using fluorobenzene as an internal standard. See supplementary materials for experimental details. (**A**) Percentage of VDF delivered to solution (determined by ^{19}F NMR) from freshly prepared VDF-Mg$_2$(dobdc) or wax-encapsulated VDF-Mg$_2$(dobdc). Ph, phenyl. (**B**) Scope of Pd-catalyzed defluorinative coupling of VDF and (hetero)arylboronic acids using VDF-Mg$_2$(dobdc). ^{19}F NMR yields are given with isolated yields shown in parentheses. For the reactions corresponding to the yields in the first row, VDF-Mg$_2$(dobdc) was freshly prepared and dispensed using a solid-addition funnel. For the reactions corresponding to the yields in the second row, VDF-Mg$_2$(dobdc) wax capsules were stored on the benchtop for 24 hours before they were broken to dispense VDF-Mg$_2$(dobdc). R, functional group. (**C**) Pd-catalyzed defluorinative coupling of HFP and arylboronic acids using HFP-Mg$_2$(dobdc). (**D**) Performance of VDF-Mg$_2$(dobdc) in defluorinative coupling with 4-biphenylboronic acid after storage under different conditions. An asterisk indicates that the wax capsule was cut open before dispensing VDF-Mg$_2$(dobdc); a dash indicates not determined.

Long-term stability of gas-MOF reagents

To probe the long-term storability of gas-Mg$_2$(dobdc) reagents, we evaluated their performance in the defluorinative coupling of VDF and 4-biphenylboronic acid after storage under different conditions for up to 2 months (Fig. 3D). Bulk samples of VDF-Mg$_2$(dobdc) can be stored at –30°C under an inert atmosphere or at –20°C in air for up to 7 days with negligible loss in performance; only a minor decrease in yield was observed after storage for 14 days (glovebox and lab freezer in Fig. 3D and table S32). Storage of VDF-Mg$_2$(dobdc) in a desiccator at RT for 1 day resulted in the same yield as standard conditions, whereas storage in a desiccator for up to 1 week still afforded the product in good yield (desiccator in Fig. 3D and table S32). Leaving VDF-Mg$_2$(dobdc) on the benchtop in air at RT overnight before adding it to the reaction also produced a good yield of product (table S31, entry 3). Together, these results suggest that slow gas loss from bulk VDF-Mg$_2$(dobdc) is largely driven by entropic effects and that gas-MOF reagents are stable under ambient conditions as long as they are kept cold. To further improve the long-term stability and safety of the gas-MOF reagents at RT, we evaluated whether storage within wax capsules arrests gas loss under ambient conditions. Indeed, storage of VDF-Mg$_2$(dobdc) in a wax capsule on the benchtop at RT for 2 months before adding it to the reaction produced a comparable yield to that obtained using freshly prepared VDF-Mg$_2$(dobdc) (wax capsule in Fig. 3D and table S32). Either adding the wax capsule directly (followed by sonication) or cutting it open to dispense VDF-Mg$_2$(dobdc) to the reaction mixture resulted in similar yields of the product. As such, wax-encapsulated gas-Mg$_2$(dobdc) represents a benchstable reagent for gas delivery on demand and provides a safer alternative to handling the gas-MOF powder directly.

Further synthetic applications

Beyond functionalizing the C–F bond of VDF to produce α-fluorostyrenes, we envisaged diversification of the C–H bond to produce β,β-difluorostyrenes as well. *Gem*-difluoroalkenes are of particular interest in medicinal chemistry because they are bioisosteres for carbonyl groups (*4*, *6*, *48*–*50*). For example, the antimalarial

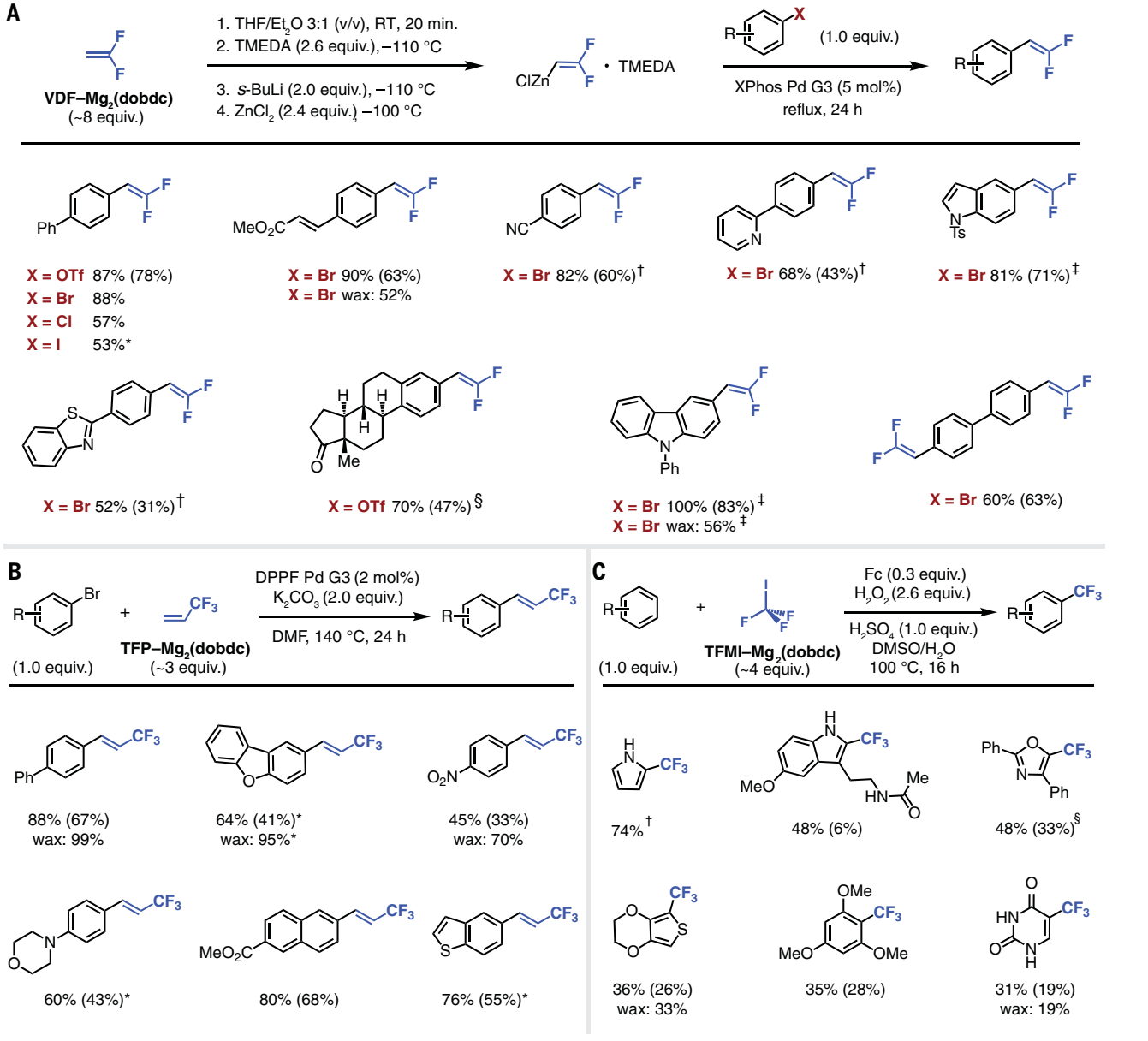

Fig. 4. Generalizability of gas-MOF delivery. ^{19}F NMR yields are given with isolated yields shown in parentheses. NMR yields were determined by ^{19}F NMR spectroscopy using fluorobenzene as an internal standard. See supplementary materials for experimental details. For the reactions corresponding to the yields in the first row, gas-Mg_2(dobdc) was freshly prepared and dispensed using a solid-addition funnel. For the reactions corresponding to the yields in the second row, gas-Mg_2(dobdc) wax capsules were stored on the benchtop for 24 hours before they were broken to dispense gas-Mg_2(dobdc). (**A**) Scope of Negishi coupling of (hetero)aryl halides and VDF-ZnCl•TMEDA synthesized from VDF-Mg_2(dobdc). OTf, trifluoromethanesulfonate; *s*-BuLi, *sec*-butyllithium; Ts, *p*-toluenesulfonyl. *$Pd(PPh_3)_4$; †8 hours, 10 mol % XPhos Pd G3; ‡18 hours, 10 mol % XPhos Pd G3; §11 hours, 10 mol % XPhos Pd G3. (**B**) Scope of Pd-catalyzed Heck coupling of (hetero)aryl bromides and TFP using TFP-Mg_2(dobdc). *XantPhos Pd G3 (2 mol %) and tetrabutylammonium bromide (1 equivalent). (**C**) Scope of Fe-catalyzed trifluoromethylation of (hetero)arenes using TFMI-Mg_2(dobdc). Fc, ferrocene. †0.15 mmol $FeSO_4{\cdot}7H_2O$ (0.3 equivalents), 50°C; §50°C.

activity of artemisinin can be improved by replacing the ester carbonyl group with a *gem*-difluoroalkene (*4*). Standard protocols to install *gem*-difluoroalkenes via carbonyl olefination reactions or defluorination of trifluoromethylated alkenes involve the use of complex starting materials or reagents and suffer from poor selectivity or modest scopes owing to the harsh reaction conditions (*51*–*57*). The development of cross-coupling methods has led to *gem*-difluorovinylating reagents, including 2,2-difluorovinyl pinacolboranes (*58*), 2,2-difluorovinylstannanes (*59*, *60*), and 2,2-difluorovinyl tosylates (*61*, *62*). However, these reagents are not bench stable, and their preparation entails complex synthesis and isolation procedures. As such, access to β,β-difluorostyrene analogs directly from readily available (hetero)aryl halides and VDF represents a desirable transformation. We used VDF-Mg_2(dobdc) to prepare 2,2-difluorovinylzinc chloride–*N*,*N*,*N*′,*N*′-tetramethylenediamine (VDF-ZnCl•TMEDA), which can be engaged in Pd-catalyzed Negishi couplings with (hetero)aryl halides to yield β,β-difluorostyrenes (*63*) (Fig. 4A). A brief reaction optimization revealed that the combination of VDF-ZnCl•TMEDA and catalytic amounts of XPhos Pd G3 (see fig. S1 for structure) in THF and Et_2O (Et_2O is diethyl ether) at reflux affords the β,β-difluorostyrene products from (hetero)aryl bromides in excellent

yields (table S27, entry 3). Notably, despite exposure to strongly nucleophilic and basic conditions, Mg_2(dobdc) retains its crystallinity after the reaction (fig. S95). Moreover, a variety of electrophilic functional groups (esters, nitriles, ketones) are compatible with this protocol, and they do not undergo nucleophilic attack by the organozinc reagent. Further, difluorovinyl groups can be successfully installed onto substrates containing *N*-heterocycles (pyridine, carbazole, indole, and thiazole) as well as biologically active molecules (estrone). Finally, this procedure can be extended to achieve a double coupling with an aryl dibromide, which produces the bis(difluorovinyl)ated product in good yield. Even with the use of air-sensitive reagents to generate VDF-ZnCl•TMEDA, delivery of VDF-Mg_2(dobdc) from day-old wax capsules results in comparable yields. The developed method represents a general approach to prepare β,β-difluorostyrenes under mild conditions.

We sought to further explore the generality of our delivery strategy by using Mg_2(dobdc) to deliver other fluorinated gases, namely TFP and TFMI. Similar to fluoroalkenes, trifluoromethylated alkenes have been used as amide mimics in medicinal chemistry (*64*). Conventionally, β-trifluoromethylstyrenes are constructed via the transition metal–catalyzed trifluoromethylation of β-halostyrenes (*65*); however, the lack of available β-halostyrene substrates severely limits the reaction scope. Previously reported Pd-catalyzed Heck reactions of TFP and aryl halides suffer from long reaction times, dependence on specialized equipment (e.g., high-pressure reactor autoclaves), the need to generate TFP in situ, and/or limited scopes (*16*, *66*). Building on these precedents, we used TFP-Mg_2(dobdc) reagents to deliver TFP for Heck coupling reactions with electronically diverse (hetero)aryl bromides to access a broad scope of β-trifluoromethylstyrenes (Fig. 4B). We investigated the Pd-catalyzed reaction of 4-bromobiphenyl with TFP under standard Heck coupling conditions using palladium acetate [$Pd(OAc)_2$] as the catalyst, potassium carbonate (K_2CO_3) as the base, and DMF as the solvent at 150°C, which afforded the β-trifluoromethylstyrene product in 17% yield (table S28, entry 1). During an investigation of a variety of Pd catalysts, we found that the use of DPPF Pd G3 (see fig. S1 for structure) leads to synthetically useful yields (table S28, entry 3). Although electron-neutral and -deficient aryl bromides react efficiently under these conditions, electron-rich derivatives exhibit sluggish reactivity. The simplicity of working with TFP-Mg_2(dobdc) enabled us to quickly survey different Pd catalysts and discover that the use of XantPhos Pd G3 (see fig. S1 for structure) in conjunction with tetrabutylammonium bromide (TBAB) as a phase transfer catalyst leads to improved yields for these challenging substrates (table S29, entry 6). With optimized conditions in hand, we expanded the reaction scope to an array of (hetero)aryl bromides bearing a variety of functional groups, which furnished the β-trifluoromethylstyrene products in good yields (Fig. 4B). Similar to VDF-Mg_2(dobdc), other gas-MOF reagents can be stored in wax capsules for 24 hours on the benchtop before use. Delivery of TFP-Mg_2(dobdc) from wax capsules results in excellent yields of β-trifluoromethylstyrenes.

We next used TFMI-Mg_2(dobdc) reagents to introduce valuable trifluoromethyl groups into (hetero)aromatic compounds (Fig. 4C). Trifluoromethyl groups are common in drugs (*67*) and appear in ~19% of fluorinated pharmaceuticals (*68*). TFMI represents an inexpensive and safe reagent for generating trifluoromethyl radicals (*17*, *69*–*72*). Compared with traditional Ru-based (*71*, *72*) or Ir-based (*70*) photoredox catalysis, Fe salts (*69*) are inexpensive potential catalysts for oxidatively generating trifluoromethyl radicals from TFMI under Fenton-like conditions without the need for complicated reaction setups or light irradiation. As such, we focused on developing a general procedure for radical, Minisci-like (hetero)arene trifluoromethylation using Fe catalysts. A brief optimization using uracil as the model substrate revealed that the combination of TFMI-Mg_2(dobdc), ferrocene, hydrogen peroxide (H_2O_2), and sulfuric acid (H_2SO_4) in dimethyl sulfoxide (DMSO) and H_2O at 100°C affords the trifluoromethylated product in good yield (table S30, entry 3). These conditions can be applied to a variety of substrates, including five-membered heteroarenes (pyrrole, indole, oxazole) and biologically active molecules (melatonin and uracil). Delivery of TFMI-Mg_2(dobdc) from wax capsules leads to similar yields as those obtained under standard conditions. Although the major product is accompanied by trifluoromethylation at other positions, isolation of the desired isomer in every case is possible with flash chromatography.

Collectively, we have demonstrated that gas-Mg_2(dobdc) reagents can be handled as free-flowing solids and used under synthetically relevant conditions to streamline a series of fluorovinylation and trifluoromethylation reactions. The bulk gas-Mg_2(dobdc) solids can be stored long-term (at low temperatures) for use in multiple reactions on different days or embedded within wax capsules to produce safer, indefinitely bench-stable reagents. Because gas-MOF powders are prone to slow gas loss over time, they should be generated on-site before use. As a safer option, we expect that wax-encapsulated gas-MOF reagents will be more widely adopted by synthetic chemists who are interested in reaction development using fluorinated gaseous reagents. Although we focus on fluorinated gases in this work, this strategy can, in principle, be generalized to the practical delivery of other gaseous reagents of interest to synthetic organic and medicinal chemists. We expect that these stable gas-MOF reagents will streamline the optimization of a myriad of transformations.

REFERENCES AND NOTES

1. E. P. Gillis, K. J. Eastman, M. D. Hill, D. J. Donnelly, N. A. Meanwell, *J. Med. Chem.* **58**, 8315–8359 (2015).
2. T. Fujiwara, D. O'Hagan, *J. Fluor. Chem.* **167**, 16–29 (2014).
3. Y. Asahina, K. Iwase, F. Iinuma, M. Hosaka, T. Ishizaki, *J. Med. Chem.* **48**, 3194–3202 (2005).
4. G. Magueur, B. Crousse, M. Ourévitch, D. Bonnet-Delpon, J.-P. Bégué, *J. Fluor. Chem.* **127**, 637–642 (2006).
5. J.-P. Bégué, D. Bonnet-Delpon, *ChemMedChem* **2**, 608–624 (2007).
6. M. Bobek, I. Kavai, E. De Clercq, *J. Med. Chem.* **30**, 1494–1497 (1987).
7. R. Halder, T. Ritter, *J. Org. Chem.* **86**, 13873–13884 (2021).
8. S. Caron, *Org. Process Res. Dev.* **24**, 470–480 (2020).
9. R. Szpera, D. F. J. Moseley, L. B. Smith, A. J. Sterling, V. Gouverneur, *Angew. Chem. Int. Ed.* **58**, 14824–14848 (2019).
10. T. Liang, C. N. Neumann, T. Ritter, *Angew. Chem. Int. Ed.* **52**, 8214–8264 (2013).
11. C. S. Shultz, S. W. Krska, *Acc. Chem. Res.* **40**, 1320–1326 (2007).
12. M. Shevlin, *ACS Med. Chem. Lett.* **8**, 601–607 (2017).
13. G. J. M. Velders, D. W. Fahey, J. S. Daniel, M. McFarland, S. O. Andersen, *Proc. Natl. Acad. Sci. U.S.A.* **106**, 10949–10954 (2009).
14. N.-F. K. Kaiser, A. Hallberg, M. Larhed, *J. Comb. Chem.* **4**, 109–111 (2002).
15. J. Demaerel, C. Veryser, W. M. De Borggraeve, *React. Chem. Eng.* **5**, 615–631 (2020).
16. G. K. S. Prakash, H. S. Krishnan, P. V. Jog, A. P. Iyer, G. A. Olah, *Org. Lett.* **14**, 1146–1149 (2012).
17. F. Sladojevich, E. McNeill, J. Börgel, S.-L. Zheng, T. Ritter, *Angew. Chem. Int. Ed.* **54**, 3712–3716 (2015).
18. H. Furukawa, K. E. Cordova, M. O'Keeffe, O. M. Yaghi, *Science* **341**, 1230444 (2013).
19. H. Li *et al*., *Mater. Today* **21**, 108–121 (2018).
20. P. Kittikhunnatham *et al*., *Angew. Chem. Int. Ed.* **61**, e202113909 (2022).
21. Ü. Kökçam-Demir *et al*., *Chem. Soc. Rev.* **49**, 2751–2798 (2020).
22. M. E. Zick *et al*., *J. Am. Chem. Soc.* **143**, 1948–1958 (2021).
23. J. Zheng *et al*., *J. Am. Chem. Soc.* **142**, 3002–3012 (2020).
24. S. R. Caskey, A. G. Wong-Foy, A. J. Matzger, *J. Am. Chem. Soc.* **130**, 10870–10871 (2008).
25. S. S.-Y. Chui, S. M.-F. Lo, J. P. H. Charmant, A. G. Orpen, I. D. Williams, *Science* **283**, 1148–1150 (1999).
26. P. Horcajada *et al*., *Chem. Commun.* **2007**, 2820–2822 (2007).
27. P. Serra-Crespo, E. V. Ramos-Fernandez, J. Gascon, F. Kapteijn, *Chem. Mater.* **23**, 2565–2572 (2011).
28. N. L. Rosi *et al*., *J. Am. Chem. Soc.* **127**, 1504–1518 (2005).
29. M. T. Kapelewski *et al*., *J. Am. Chem. Soc.* **136**, 12119–12129 (2014).
30. Z. Wang, A. Bilegsaikhan, R. T. Jerozal, T. A. Pitt, P. J. Milner, *ACS Appl. Mater. Interfaces* **13**, 17517–17531 (2021).
31. A. C. Forse, J. M. Griffin, V. Presser, Y. Gogotsi, C. P. Grey, *J. Phys. Chem. C* **118**, 7508–7514 (2014).
32. A. C. Sather, H. G. Lee, J. R. Colombe, A. Zhang, S. L. Buchwald, *Nature* **524**, 208–211 (2015).
33. M. Drouin, J.-D. Hamel, J.-F. Paquin, *Synthesis* **50**, 881–955 (2018).
34. M. Drouin, J.-F. Paquin, *Beilstein J. Org. Chem.* **13**, 2637–2658 (2017).
35. J. J. Urban, B. G. Tillman, W. A. Cronin, *J. Phys. Chem. A* **110**, 11120–11129 (2006).
36. S. Couve-Bonnaire, D. Cahard, X. Pannecoucke, *Org. Biomol. Chem.* **5**, 1151–1157 (2007).
37. K. Matsuda, J. A. Sedlak, J. S. Noland, G. C. Gleckler, *J. Org. Chem.* **27**, 4015–4020 (1962).
38. H. Suga, T. Hamatani, Y. Guggisberg, M. Schlosser, *Tetrahedron* **46**, 4255–4260 (1990).
39. J. R. McCarthy, D. P. Matthews, C. L. Barney, *Tetrahedron Lett.* **31**, 973–976 (1990).
40. J. Qiu, A. Gyorokos, T. M. Tarasow, J. Guiles, *J. Org. Chem.* **73**, 9775–9777 (2008).
41. T. Hanamoto, T. Kobayashi, M. Kondo, *Synlett* **2001**, 0281–0283 (2001).

42. T. Hanamoto, T. Kobayashi, *J. Org. Chem.* **68**, 6354–6359 (2003).
43. W. Heitz, A. Knebelkamp, *Makromol. Chem., Rapid. Commun.* **12**, 69–75 (1991).
44. A. Knebelkamp, W. Heitz, *Makromol. Chem., Rapid. Commun.* **12**, 597–606 (1991).
45. C. A. Malapit, J. R. Bour, C. E. Brigham, M. S. Sanford, *Nature* **563**, 100–104 (2018).
46. W. Dmowski, *J. Fluor. Chem.* **18**, 25–30 (1981).
47. M. Ohashi, H. Saijo, M. Shibata, S. Ogoshi, *Eur. J. Org. Chem.* **2013**, 443–447 (2013).
48. C. Leriche, X. He, C. W. Chang, H. W. Liu, *J. Am. Chem. Soc.* **125**, 6348–6349 (2003).
49. J.-M. Altenburger *et al*., *Bioorg. Med. Chem.* **12**, 1713–1730 (2004).
50. S. Messaoudi *et al*., *J. Med. Chem.* **52**, 4538–4542 (2009).
51. X. Zhang, S. Cao, *Tetrahedron Lett.* **58**, 375–392 (2017).
52. B. Gao, Y. Zhao, M. Hu, C. Ni, J. Hu, *Chemistry* **20**, 7803–7810 (2014).
53. I. Nowak, M. J. Robins, *Org. Lett.* **7**, 721–724 (2005).
54. Y. Huang, T. Hayashi, *J. Am. Chem. Soc.* **138**, 12340–12343 (2016).
55. J. P. Phelan *et al*., *J. Am. Chem. Soc.* **141**, 3723–3732 (2019).
56. J. Ichikawa, *J. Synth. Org. Chem. Jpn.* **68**, 1175–1184 (2010).
57. J. Zhang, J.-D. Yang, J.-P. Cheng, *Nat. Commun.* **12**, 2835 (2021).
58. O. P. Blahun *et al*., *Eur. J. Org. Chem.* **2019**, 6417–6421 (2019).
59. L. Lu, D. J. Burton, *J. Fluor. Chem.* **133**, 16–19 (2012).
60. S. Y. Han, I. H. Jeong, *Org. Lett.* **12**, 5518–5521 (2010).
61. T. M. Gøgsig, L. S. Søbjerg, A. T. Lindhardt, K. L. Jensen, T. Skrydstrup, *J. Org. Chem.* **73**, 3404–3410 (2008).
62. B. Xiong *et al*., *ACS Catal.* **10**, 13616–13623 (2020).
63. T. Fujita, T. Ichitsuka, K. Fuchibe, J. Ichikawa, *Chem. Lett.* **40**, 986–988 (2011).
64. J. Xiao, B. Weisblum, P. Wipf, *J. Am. Chem. Soc.* **127**, 5742–5743 (2005).
65. T. Kitazume, N. Ishikawa, *J. Am. Chem. Soc.* **107**, 5186–5191 (1985).
66. T. Fuchikami, M. Yatabe, I. Ojima, *Synthesis* **1981**, 365–366 (1981).
67. A. S. Nair *et al*., *Processes* **10**, 2054 (2022).
68. M. Inoue, Y. Sumii, N. Shibata, *ACS Omega* **5**, 10633–10640 (2020).
69. T. Kino *et al*., *J. Fluor. Chem.* **131**, 98–105 (2010).
70. D. A. Nagib, M. E. Scott, D. W. C. MacMillan, *J. Am. Chem. Soc.* **131**, 10875–10877 (2009).
71. P. V. Pham, D. A. Nagib, D. W. C. MacMillan, *Angew. Chem. Int. Ed.* **50**, 6119–6122 (2011).
72. Y. Ye, M. S. Sanford, *J. Am. Chem. Soc.* **134**, 9034–9037 (2012).
73. J. A. Mason, M. Veenstra, J. R. Long, *Chem. Sci.* **5**, 32–51 (2014).
74. W. L. Queen *et al*., *J. Phys. Chem. C* **115**, 24915–24919 (2011).

ACKNOWLEDGMENTS

Computational resources provided by the KISTI Supercomputing Center (project no. KSC-2020-CRE-0361) are gratefully acknowledged (J.-H.L.). This work made use of the Cornell Center for Materials Research Shared Facilities, which are supported through the NSF MRSEC program (DMR-1719875). NMR data were collected on a Bruker INOVA 500-MHz spectrometer that was purchased with support from the NSF (CHE-1531632). We are grateful for the resources provided by the Advanced Photon Source, which is supported by the US Department of Energy, Office of Science, Office of Basic Energy Sciences, under contract no. DE-AC02-06CH11357. We thank the Cornell University Glass Shop for providing the custom-built, solid-addition funnels used in this work. We thank S. Meng, T. Hyster, T. Lambert, and S. Lin (Cornell University) for editorial assistance during the preparation of this manuscript. **Funding:** This work was funded by Cornell University (K.T.K., M.E.Z., E.E.S., J.K., P.J.M.); the National Institute of General Medical Sciences of the National Institutes of Health (R35GM138165) (K.T.K., M.E.Z., E.E.S., J.K., P.J.M.); a Bristol Myers Squibb fellowship (K.T.K.); the KIST Institutional Program (project no. 2E31801) (J.-H.L.); the National Center for Materials Research Data (NCMRD) through the National Research Foundation of Korea funded by the Ministry of Science and ICT (2021M3A7C2089739) (J.-H.L.); the NSF (CHE-1531632); the NSF MRSEC program (DMR-1719875); the Robert A. Welch Foundation (grant no. N-2012-20220331) (L.A., T.R.); the US Department of Energy, Office of Science, Office of Basic Energy Sciences (DE-AC02-06CH11357); and a Camille Dreyfus Teacher-Scholar Award (TC-23-048) (P.J.M.). The content is solely the responsibility of the authors and does not necessarily represent the official views of the National Institutes of Health. **Author contributions:** Conceptualization: P.J.M., K.T.K., M.E.Z., E.E.S.; Methodology: K.T.K., M.E.Z., E.E.S., J.K., J.-H.L., L.A.; Investigation: K.T.K., M.E.Z., E.E.S., J.K., J.-H.L., L.A.; Visualization: P.J.M., K.T.K., M.E.Z., E.E.S.; Funding acquisition: P.J.M., J.-H.L., T.R.; Project administration: P.J.M., J.-H.L., T.R.; Supervision: P.J.M., T.R.; Writing – original draft: K.T.K., P.J.M.; Writing – review and editing: K.T.K., M.E.Z., E.E.S., J.K., J.-H.L., L.A., T.R., P.J.M. **Competing interests:** P.J.M., K.T.K., and M.E.Z. are listed as inventors on a patent that includes gas-reagent delivery using MOFs (Cornell University, international patent application no. PCT/US2023/019456, filed 21 April 2023). **Data and materials availability:** All data are available in the main text or the supplementary materials.

SUPPLEMENTARY MATERIALS

science.org/doi/10.1126/science.adg8835
Materials and Methods
Supplementary Text
Figs. S1 to S181
Tables S1 to S32
References (*75*–*113*)

Submitted 27 January 2023; resubmitted 12 June 2023
Accepted 24 August 2023
10.1126/science.adg8835